# Harvesting $^{62}$Zn from an aqueous cocktail at the NSCL

| | |
|---|---|
| Journal: | *New Journal of Chemistry* |
| Manuscript ID | NJ-ART-09-2020-004411.R1 |
| Article Type: | Paper |
| Date Submitted by the Author: | 02-Nov-2020 |
| Complete List of Authors: | Domnanich, Katharina; Michigan State University, Chemistry; Michigan State University, Facility for Rare Isotope Beams<br>Vyas, Chirag; Michigan State University, Chemistry; Michigan State University, Facility for Rare Isotope Beams<br>Abel, E. Paige; Michigan State University, Chemistry; Michigan State University, Facility for Rare Isotope Beams<br>Kalman, Colton; Michigan State University, Chemistry; Michigan State University, Facility for Rare Isotope Beams<br>Walker, Wesley; Michigan State University, Chemistry; Michigan State University, Facility for Rare Isotope Beams<br>Severin, Gregory; Michigan State University, Chemistry; Michigan State University, Facility for Rare Isotope Beams |
| | |

# Harvesting $^{62}$Zn from an aqueous cocktail at the NSCL

Katharina A. Domnanich[1,2], Chirag K. Vyas[1,2], E. Paige Abel[1,2], Colton Kalman[1,2], Wesley Walker[1,2], Gregory W. Severin[1,2]

[1] Department of Chemistry, Michigan State University, 578 S Shaw Ln, East Lansing, MI 48824, USA

[2] National Superconducting Cyclotron Laboratory, Michigan State University, 640 S Shaw Ln, East Lansing, MI 48824, USA

e-mail addresses

domnanic@frib.msu.edu, vyas@frib.msu.edu, abelp@nscl.msu.edu, kalman@nscl.msu.edu, walkerw@frib.msu.edu, severin@frib.msu.edu

* Corresponding author

Gregory W. Severin

National Superconducting Cyclotron Laboratory

Michigan State University

640 S. Shaw Ln

East Lansing, MI 48824, USA

e-mail: severin@frib.msu.edu

phone:+1-517-353-1087

## Abstract

"Isotope harvesting" is a technique that offers access to exotic radionuclides created as by-products during nuclear science research. Ongoing exploratory work at the National Superconducting Cyclotron Laboratory (NSCL) is directed towards the production and extraction of rare radionuclides from a flowing-water target and intends to pave the way for future harvesting efforts at the upcoming Facility for Rare Isotope Beams (FRIB). Here we present the collection of $^{62}$Zn from an aqueous matrix irradiated with a 150 MeV/nucleon $^{78}$Kr beam, while synergistically capturing other gaseous reaction products. In addition to the production rate for $^{62}$Zn (9.08(30)E-5 $^{62}$Zn per incoming $^{78}$Kr), the rates of formation for several other radionuclides were determined as well. The purification of $^{62}$Zn from a large number of co-produced radionuclides was performed by anion exchange chromatography, allowing the isolation of 80.5(5.2) % of the generated $^{62}$Zn. With the decay of $^{62}$Zn the radioactive daughter $^{62}$Cu is generated, and with the isolation of pure $^{62}$Cu eluate, the principle of a medical radionuclide generator could be demonstrated. To illustrate the applicability of the obtained $^{62}$Zn, the isolated product was used in free and DTPA-labelled form in a proof of principle plant uptake study with garden cress employing phosphor imaging for visualization.

## Introduction

At the NSCL the production of radioactive secondary beams for nuclear physics experiments is achieved by the acceleration of stable heavy ions. However, this process only utilizes a small fraction of the primary beam, and the unreacted majority is separated and finally stopped in a solid block of tungsten. Rather than discarding the beam in this way, the tungsten block can be replaced by a water-filled target. There, interactions between the incoming particle beam and the nuclei of the water molecules produce a variety of by-product radionuclides. The collection of these radioactive species has been termed "isotope harvesting" and was initially realized by irradiating water samples in a batch-wise manner. After irradiation, the selected radionuclides could be extracted in a chemically pure form. This setup was successfully used for the collection of $^{24}$Na, $^{48}$V and $^{67}$Cu, before switching to a flowing-water irradiation target. Such a system allows for higher beam powers, and for the radionuclides to be extracted online as successfully demonstrated with $^{40}$Ca and $^{48}$Ca.[1–7] Through isotope harvesting, a unique and yet untapped source of rare radionuclides becomes accessible to help meet the increasing demands for radionuclides in various disciplines, among them astrophysics, material science, medicine, plant biology and stockpile stewardship science. With the high-power beams of the upcoming FRIB, isotope harvesting will enable the collection of unprecedented amounts of these radionuclides in a synergistic manner with nuclear physics experiments.[2]

As a part of the experimental program leading up to isotope harvesting at FRIB, a $^{78}$Kr$^{35+}$ primary particle beam was used to irradiate the water-filled beam blocker at the NSCL. When a $^{78}$Kr beam is stopped in the water matrix, the main nuclear reaction products are $^{77}$Kr and $^{76}$Kr. These are valuable radionuclides for tracing the behaviour of dissolved gases in the beam-water system and to generate medically relevant radio-bromine.[8,9] (the results of gas-phase harvesting will be discussed in a separate manuscript). However, there are numerous other radionuclides formed in the beam blocker that are worthwhile to harvest. One key element of the isotope harvesting concept is to be able to attain multiple radionuclides simultaneously, and for the current work co-produced $^{62}$Zn was selected to demonstrate the feasibility of commensurate harvesting with the krypton isotopes.

The positron emitter $^{62}$Zn ($t_{1/2}$= 9.2h) is the radioactive parent of the medically relevant, short-lived copper isotope $^{62}$Cu ($t_{1/2}$= 9.7 min, $E\beta^{+}_{av}$= 1.3 MeV, $I\beta^{+}_{av}$= 97.6%), making it a useful co-harvesting target.[10,11] The equilibrium composition of the $^{62}$Zn/$^{62}$Cu pair is known as a radionuclide generator, and it allows multiple separations of $^{62}$Cu over extended time periods. In nuclear medicine the short half-life of $^{62}$Cu is well suited for Positron Emission Tomography (PET) imaging of tissue hypoxia and to quantify the blood flow in organs. In combination with its therapeutic counterparts, $^{64}$Cu and $^{67}$Cu, the radioisotopes of Cu epitomize a ‘matched pair’ with suitable characteristics for theragnostic applications.[12–14] The development of a $^{62}$Zn/$^{62}$Cu generator was addressed in numerous studies, and most systems are based on the strong adsorption of $^{62}$Zn on anion exchange resin, while isolating $^{62}$Cu with a low molarity HCl eluent or a mixture of NaCl and HCl.[15–18]

In addition to generating $^{62}$Cu, $^{62}$Zn is also interesting as a radiotracer for zinc in plant biology. Zinc represents an essential micronutrient for plant growth and development, and it is an integral component of numerous plant proteins and regulatory cofactors in enzymes. Zinc deficiency has become a major agricultural problem with far-reaching consequences for human health.[19,20] Keeping this in mind, studies towards elucidating the role of zinc in metabolomic processes of various plants are of great importance. The suitable decay characteristics of $^{62}$Zn would render this radiometal as an alternative possibility in metabolomics experiments. Ideally, isotope harvesting will increase the availability of $^{62}$Zn for use in plant biology studies.

In the present study, the formation of $^{62}$Zn in a water matrix by irradiation with a $^{78}$Kr beam, and its subsequent collection on a cation exchange column were demonstrated and characterized. The feasibility of collecting a by-product radioactive ion from the aqueous phase simultaneously with the main gaseous products has been demonstrated. The production rates of various other in-beam produced radionuclides were determined and compared with theoretical predictions. After successful chromatographic separation of $^{62}$Zn from co-produced radionuclides, the radioactive decay of $^{62}$Zn was utilized to generate $^{62}$Cu in a pure form. The isolated $^{62}$Zn was also directly used in ligand-free and DTPA-radiolabelled form in a proof-of-principle uptake and imaging study with a hydroponic garden cress culture.

# Experimental

## Experimental setup and Isotope harvesting system

The heavy ion irradiations were performed at the NSCL with a $^{78}$Kr primary beam, accelerated to an energy of 150 MeV/nucleon by the Coupled Cyclotron Facility. To extract the pure primary beam, the beryllium target typically used for fragmentation of the beam was removed and the A1900 projectile fragment separator was set in a way to select only one charge state which was finally directed towards the flowing-water target. A combination of the beam current information from calibrated and suppressed Faraday cups was used to quantify the amount of $^{78}$Kr particles delivered to the flowing-water target. The resulting linear relationship of the signals was used to scale the beam intensity measured at the flowing-water target. During two irradiation experiments, performed in April and May 2019, the beam currents were ramped up steadily, resulting in intensities of 0.3–3.7 pnA (table 1). Note: the unit *pnA* is used to denote particle-nanoAmperes, which is the electrical current in nA divided by the beam's charge state. One pnA is equivalent to 6.2E9 particles per second.

**Table 1** Summary of the irradiation conditions during the $^{78}$Kr beam experiment

| Experiment | | Charge state on target | Beam current [pnA] | Beam power [W] | Irradiation time [min] |
|---|---|---|---|---|---|
| 1 | April 2019 | 36+ | 0.3–2.2 | 2.0–14.9 | 332 |
| 2 | May 2019 | 35+ | 1.3–3.7 | 8.7–25.1 | 469 |

The flowing water target was installed at the end of an experimental beamline after a 75 µm thick zirconium window (used to isolate the beamline vacuum from the target chamber).[26] The shell of the flowing-water target consists of 3D-printed titanium alloy (Ti64, 90% Ti, 6% Al, 4%V, Stratasys, Minneapolis MN, USA) and the design facilitates the flow of water through the integrated channels. When the $^{78}$Kr beam impacted on the double-walled Ti64 front window, it completely traversed the first water channel and was stopped in the second, larger cavity. A detailed description of the beam blocker is given elsewhere[4] and the passage of the $^{78}$Kr beam through the target is shown in the Supplementary Information, Fig. S1.

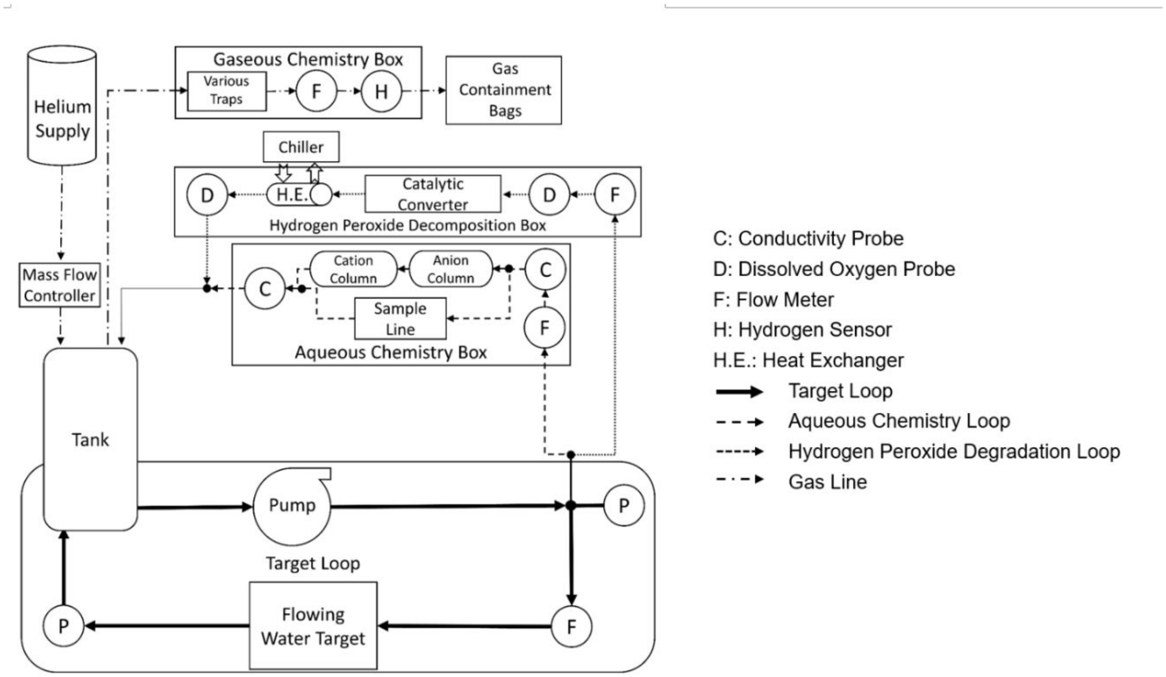

**Fig. 1** Schematic diagram of the isotope harvesting system

As the beam particles traverse the water, nuclear reactions are induced, thereby creating a variety of different radionuclides. The active collection of the generated radioactive species is facilitated by an isotope harvesting system, designed and successfully implemented for irradiation experiments at the NSCL.[4] An overview of the system is provided by the schematic in Fig. 1.

In brief, the core element is represented by the flowing-water target, where the radionuclides were created and transported away by the fast water flow (~10 L/min). The total system encompasses a volume of up to 36 L water which was moved by a pump from the storage tank through multiple loops. In the aqueous chemistry box, the water was sequentially passed over an anion and then over a cation exchange column at a flow rate of ~300 mL/min to collect all stable and radioactive ionic species. Each column contained 1.5 g of anion (in $OH^-$ form, BioRad AG 1x8, 20–50 mesh) or cation exchange resin (in $H^+$ form, BioRad AG 50W-8, 20–50 mesh) immobilized against the pressure of the flowing water by small amounts of glass wool on top and bottom. Parallel to the array of ion exchange columns, a sampling line facilitated the withdrawal of water samples. Temporary suspensions of the irradiation allowed for water sampling and to replace the ion chromatography resin beds. For each irradiation experiment two sets of resins, with one cation and one anion exchange resin beds each, were employed. With a post-irradiation collection time of 5.8 and 9.7 hours, an exhaustive capturing of the generated radionuclides from the water was achieved.

With a helium-based purge-gas stream flowing through the water in the tank, gaseous species were transferred from the water into the tank headspace and captured on a variety of further downstream placed traps. To mitigate the hydrogen peroxide levels, one of the long-lived radiolysis products, a fraction of the water flow was directed over a catalytic converter.[27] To maintain a temperature between 15°C and

25°C, the water was passed through a heat exchanger interfaced with a chiller. A constant monitoring of the water quality was established by a set of two dissolved oxygen sensors and two conductivity probes. A hydrogen analyser placed at the end of the gaseous chemistry loop enabled the monitoring of radiolysis produced hydrogen.

**Radionuclide quantification and comparison with the estimated production**

Gamma ray spectroscopy with a Broad Energy Ge Detector (BE2020, Canberra) was employed to identify and quantify the radionuclides on many components of the harvesting systems, including the ion exchange resin beds, the water samples, the gas traps and the catalytic converter. The energy and efficiency calibration were performed with a $^{152}$Eu point source and gamma spectra were acquired at a distance of 25 and 50 cm using the Genie 2000 software (Mirion Technologies). The gamma ray energies and corresponding branching ratios used for the calculation of radioactivity are outlined in the Supplementary Information, table S1.

The determined activities were compared with the expected values, obtained by considering a beam current-dependent formation with a production rate predicted through the Particle and Heavy Ion Transport Code System (PHITS).[11] With the PHITS code, nuclear reactions between the incoming $^{78}$Kr particles and the water molecules at the high and low energy scenario, i.e. by fragmentation and fusion-evaporation, respectively, are considered. At the same time the produced ionic species are adsorbed from the system's water onto the ion exchange resin beds, which is governed by the adsorption rate, $k_{ads}$.

The measured activities of strongly adsorbed cations $^{7}$Be, $^{24}$Na, $^{28}$Mg, $^{43,43}$K, $^{61}$Cu, $^{62}$Zn, $^{80,83}$Sr, and $^{82m}$Rb on all cation exchange columns were summed and their total activities were decay corrected to the end of irradiation (EOI). In case of the radionuclide pair $^{81}$Sr and $^{81}$Rb, the decay of the parent and the consequential formation of the radioactive daughter were considered. The production rates of all afore mentioned radionuclides obtained in this way were finally adjusted by considering the adsorption behaviour on the column (described by equation 1 and 2 in the Supplementary Information). For the radionuclides which were adsorbed on at least two components of the harvesting system (i.e. cation and/or anion exchange column and catalytic converter) such as $^{44m}$Sc, $^{52}$Mn, $^{48}$V, $^{67}$Ga, $^{69}$Ge, $^{71}$As, $^{72,73}$Se, the production rates could only be approximated by summing the accumulated activities from the different media. The total activities of these radionuclides ($\Sigma A_{EOI}$) were obtained by considering the measured activities on all components of the harvesting system and were then decay corrected to EOI. To estimate the error in the production rates, the statistical uncertainties from the counting were propagated. (A more in-depth explanation about the performed calculations is given in the Supplementary Information, equation 1–5.)

**Isolation of $^{62}$Zn**

After removal of the cation exchange column from the isotope harvesting system, the resin was rinsed with 12–14 mL MilliQ $H_2O$ (Thermo Scientific MicroPure Ultrapure Water System, 18.2MΩ cm) and the adsorbed ionic species were eluted with 50–57 mL 1M HCl at a flow rate of 2 mL/min. The eluate was acidified with concentrated HCl (36.5–38.0%, ACS grade, VWR) to yield a 2M HCl solution. A glass column

(0.7 x 10 cm, Econo-column, BioRad) was filled with 2 g AG1x8 anion exchange resin (20–50 mesh, BioRad), rinsed with water and 5M HCl and conditioned with ~20 mL 2M HCl. The acidified fraction was loaded on the prepared AG1x8 column and subsequently rinsed with 10–12 mL 2M HCl to ensure a total removal of any adsorbed radionuclides other than $^{62}$Zn. The elution of the first $^{62}$Zn fraction was accomplished with 10 mL water, while the residual $^{62}$Zn activity was removed with 40–50 mL 0.001M HCl (pH~3). During the entire separation, the flow rate was kept at 1.4 mL/min. To demonstrate the elution of the generated $^{62}$Cu during the May experiment, the volume of the 2M HCl rinse step was increased up to 28 mL. The eluate was collected in 3–4 fractions and the identity of $^{62}$Cu was determined by gamma ray spectroscopy. Subsequently the purified $^{62}$Zn was eluted from the anion exchange column in the same way as described previously.

**Synthesis of $^{62}$Zn-DTPA and cress uptake study**

The first fraction of the $^{62}$Zn eluate (eluted with MilliQ $H_2O$) was combined with up to 40 mL of the second $^{62}$Zn fraction (eluted with 0.001M HCl), divided into two parts, and evaporated to dryness in a 50 mL round bottom flask on a rotary evaporator under vacuum conditions. The small amount of white-transparent residue was reconstituted in 1.4–2 mL 0.01M HCl. With the addition of 0.5M sodium acetate solution ($CH_3COONa$, >99.99%, Alfa Aesar) the pH was adjusted to 3. To only one set of $^{62}$Zn containing solutions 1 mL 1mM diethylenetriaminepentaacetic acid solution (DTPA, ≥99%, Sigma-Aldrich) was added, shaken well and incubated at room temperature for ~ 5 min. Each solution, independent of its DTPA content, was diluted to a final volume of 20 mL by the addition of filtered drinking water. The resulting formulations (pH ~6) were divided into two parts of 10 mL, where one part received 10 µL 10µM zinc chloride solution ($ZnCl_2$, ≥97%, ACS grade, Sigma-Aldrich) and the other one did not. With the described dilution scheme a set of four solutions, containing 14–81 kBq $^{62}$Zn and varying compositions of 1E-8M $ZnCl_2$ and 50µM DTPA, were created (table 2).

**Table 2** The composition of the prepared $^{62}$Zn-containing solutions (with a volume of 10mL for each one) for the incubation of garden cress

| A + Zn | A – Zn | B + Zn | B – Zn |
|---|---|---|---|
| 14–81 kBq $^{62}$Zn | 14–81 kBq $^{62}$Zn | 14–81 kBq $^{62}$Zn | 14–81 kBq $^{62}$Zn |
| 1E-8M $ZnCl_2$ | - | 1E-8M $ZnCl_2$ | - |
| 50µM DTPA | 50µM DTPA | - | - |

Glass petri dishes (diameter: 5–6 cm) were outfitted with a layer of cotton moistened with filtered drinking water. In analogy, a set of glass petri dishes was about half filled with filtered drinking water. Filtered drinking water was used to ensure optimal cultivation conditions. About 25–30 garden cress seeds (*Lepidium sativum L.*) were uniformly distributed in each of the prepared dishes. The seeds were cultivated for 5–7 days at room temperature while filtered water was added as necessary. Before incubation with the $^{62}$Zn-containing solutions (table 2), the water in the dishes was completely removed. The growth of cress seedlings in the control and sample dishes was monitored and used as an indicator for any growth impeding effects due to the addition of radioactive $^{62}$Zn.

The uptake of $^{62}$Zn was assessed by phosphor imaging with an Amersham Typhoon$^{TM}$ Biomolecular Imager (GE Healthcare, Chicago, USA) starting from 9.5 until 93 hours post-incubation. For each imaging experiment 2–3 seedlings per glass dish were removed and attached on a sheet of paper with a piece of tape. The exposure time to the film (20 x 40 cm, BAS-IP SR 2040, GE Healthcare), depended on the amount of radioactive $^{62}$Zn in the seedling and varied between 3 and 12 hours. Image acquisition was performed with the Amersham Typhoon$^{TM}$ software (version 1.1.0.7, GE Healthcare), at a pixel size of 100 and 200 µm. Using the post-processing software ImageQuant TL (version 8.2.0.0, GE Healthcare) the signal intensity was determined by defining the best fitting shape for each plant after background subtraction. The part of the plants which was in direct contact with the incubation solution (i.e. the roots) were not considered for the intensity determination. To indicate trends in the uptake of ligand-free $^{62}$Zn, the measured signal intensities of ligand-free $^{62}$Zn were divided by the sum of ligand-free and DTPA-labelled $^{62}$Zn. In this representation (in the following assigned as ‘percentage metric for $^{62}$Zn uptake’), a value of >50% indicates a preferred ligand-free $^{62}$Zn uptake, whereas a favoured $^{62}$Zn-DTPA uptake is defined by <50%. At 50%, both species, chelated and unchelated $^{62}$Zn, are absorbed to an equal extent. With such a representation, the data obtained with plants treated with ligand-free $^{62}$Zn is more strongly emphasized than data obtained with $^{62}$Zn-DTPA. The reasons for such a weighed consideration are the low measured signal intensities and associated large deviations of the $^{62}$Zn-DTPA treatment for the first time point measurements with phosphor imaging.

## Results and Discussion

### Radionuclide quantification and comparison with the estimated production

The PHITS-code was applied to predict the production rates of the radionuclides ($P_{PHITS}$) formed in fragmentation and fusion-evaporation reactions with an impinging $^{78}$Kr beam. The produced aqueous radionuclides were captured on a set of cation and anion exchange columns and the observed activities were used to compute the experimental production rates. The computation of the adsorption rates ($k_{ads}$) is based on an iterative approach which simultaneously finds values for the $k_{ads}$ and the production rates of $^{7}$Be, $^{24}$Na and $^{62}$Zn (representative cationic radionuclides) at their minimized $\chi^2$ difference between measured and calculated activities of the cation exchange columns. A more in-depth explanation is outlined in the Supplementary Information, ‘Radionuclide quantification and comparison with the estimated production’. Adsorption rates of 7.19(40)E-5 and 1.08(10)E-4 $s^{-1}$ were determined for the cation exchange column in the April and May experiment. These numbers are the result of two iteration steps, after which the value of the next computed $k_{ads}$ differed only by less than 1%. After the post end of irradiation collection time 95.6(28)% (April) and 97.2(49)% (May) of the $^{7}$Be, $^{24}$Na and $^{62}$Zn (representative cations) present in the system’s water were calculated to be trapped on the cation exchange resin.

In table 3 the predicted and determined production rates for radionuclides exclusively adsorbed on the cation exchange resin are given, whereas the measured activities can be found in the Supplementary Information, table S2. The production rates were only estimated for radionuclides which were present at levels allowing a reliable quantification. The low activities in all withdrawn water samples precluded a quantitative determination of the radionuclides in the water. However, with the applied iterative approach an accurate determination of the production rates became possible. Several radionuclides, such as $^{24}$Na, $^{28}$Mg, $^{43}$K, $^{61}$Cu, $^{62}$Zn, $^{80,83}$Sr and $^{81}$Rb, are not only generated by in-beam reactions, but also by a decaying parent radionuclide. Generally, the half-lives of the parent radionuclides are rather short (i.e. a few minutes), so that at the measurement time only the daughter radionuclides could be detected. Hence, the computed production rates of the daughter radionuclides can be considered as the sum of all possible production pathways ($P_{total}$). Additionally, the PHITS-predicted production rate for the parent radionuclides are considerably lower and therefore, are predicted to contribute in most cases only <2% to the experimentally determined $P_{total}$ for the daughter radionuclides. However, with the prolonged half-life of $^{81}$Sr ($t_{1/2}$ = 22.3 min) a simultaneous measurement of the daughter ($^{81}$Rb) and parent ($^{81}$Sr) radioactivity on the cation exchange column became possible, which allowed the estimation of both production rates. In this case the formation of the parent was predicted to occur at a comparable rate as the daughter nuclide (8.60E-5 $^{81}$Sr and 5.40E-5 $^{81}$Rb per incoming $^{78}$Kr), which could be corroborated by the experimental results (5.38(20)E-5 $^{81}$Sr and 1.49(20)E-5 $^{81}$Rb per incoming $^{78}$Kr). The generation of several radionuclides, such as $^{42,43}$K, $^{61}$Cu, $^{62}$Zn, $^{80}$Sr and $^{81}$Sr/$^{81}$Rb was determined to occur at a 1.6–8.2-times decreased rate, while a 1.4–13.9-fold increased formation was observed for $^{7}$Be, $^{24}$Na, $^{28}$Mg and $^{83}$Sr compared to the rates predicted with PHITS. A number of radionuclides, including $^{28}$Al, $^{47}$Sc, $^{60}$Cu, $^{63}$Zn, $^{66,68}$Ga and $^{79}$Rb were additionally identified on the cation exchange column (Supplementary Information, Fig. S2a). However, their low levels and/or short half-lives hampered a reliable gamma spectroscopic quantification on all withdrawn components of the harvesting system. Thus, no production rate estimations were performed for these radioactive species.

**Table 3** The determined total production rates ($P_{total}$) for radioactive species determined exclusively on the cation exchange column in comparison to the PHITS-based prediction ($P_{PHITS}$).

| Radionuclide | Production | $t_{1/2}$ daughter/parent | $P_{PHITS}$ daughter/parent | $P_{total}$ |
|---|---|---|---|---|
| | | | (nuclei/incoming $^{78}$Kr) | |
| $^{7}$Be | $^{7}$Be | 53.22 d | 2.55E-3 | 6.58(20)E-3 |
| $^{24}$Na | $^{24}$Na | 15 h | 8.03E-6 | 1.11(2)E-4 |
| | $^{24}$Ne → $^{24}$Na | 3.4 min | 1.61E-6 | |
| $^{28}$Mg | $^{28}$Mg | 20.9 h | 3.06E-6 | 7.48(60)E-6 |
| | $^{28}$Na → $^{28}$Mg | 31 ms | 5.63E-8 | |
| $^{42}$K | $^{42}$K | 12.4 h | 1.32E-4 | 1.60(10)E-5 |
| $^{43}$K | $^{43}$K | 22.3 h | 7.20E-5 | 1.78(5)E-5 |
| | $^{43}$Ar → $^{43}$K | 5.4 min | 1.48E-6 | |
| $^{61}$Cu | $^{61}$Cu | 3.3 h | 5.13E-4 | 1.15(6)E-4 |
| | $^{61}$Zn → $^{61}$Cu | 89 s | 2.86E-5 | |
| $^{62}$Zn | $^{62}$Zn | 9.2 h | 3.07E-4 | 9.08(30)E-5 |
| | $^{62}$Ga → $^{62}$Zn | 116 ms | 1.70E-6 | |
| $^{82m}$Rb | $^{82m}$Rb | 6.5 h | - | 7.44(30)E-6 |
| $^{80}$Sr | $^{80}$Sr | 1.8 h | 6.28E-5 | 2.30(20)E-5 |
| | $^{80}$Y → $^{80}$Sr | 30 s | 2.58E-6 | |
| $^{83}$Sr | $^{83}$Sr | 1.4 d | 4.83E-5 | 6.76(30)E-5 |
| | $^{83}$Y → $^{83}$Sr | 7.1 min | 1.94E-5 | |
| $^{81}$Sr | $^{81}$Sr | 22.3 min | 8.60E-5 | 5.38(20)E-5 |
| $^{81}$Rb | $^{81}$Rb | 4.6 h | 5.40E-5 | 1.49(20)E-5 * |
| | $^{81}$Sr → $^{81}$Rb | 22.3 min | 8.60E-5 | |

* The *P* for $^{81}$Rb considers only the direct production of this nuclide as the formation of the parent nuclide ($^{81}$Sr) could be obtained as well.

The radionuclides $^{44g/m}$Sc, $^{48}$V, $^{52}$Mn, $^{66,67,68}$Ga, $^{66,69}$Ge, $^{71\text{-}74}$As, $^{72,73,75}$Se and $^{74g/m,75,76,77}$Br were found on the cation and/or anion exchange column as well as on the catalytic converter. None of the previously mentioned species were exclusively adsorbed on the anion exchange column, and it is assumed that the adsorption on the catalytic converter occurs via nonspecific surface interactions at an unknown rate. Therefore, the iterative approach could not be applied and the production rates were approximated by considering the sum of activities found on all components (Supplemental Information, equation 3). The production rates of $^{44m}$Sc, $^{52}$Mn, $^{48}$V, $^{67}$Ga, $^{69}$Ge, $^{71}$As and $^{72,73}$Se were obtained in this way and are outlined in table 4. Only radionuclides which could be reliably determined by gamma spectroscopic measurements (i.e. at least one characteristic non-overlapping γ-ray) and additionally represented the radioactive daughter of a short-lived parent or a sufficiently long-lived parent radionuclide, were considered. The determined production rates of the daughter radionuclides can be considered as the sum of all possible formation pathways ($P_{total}$). Radioactive daughters of parent radionuclides, where both had sufficiently long half-lives to allow a simultaneous determination, were not included. With the unknown adsorption rate of the catalytic converter the source of the radioactive daughters, i.e. from direct adsorption or from the decay of the immobilized parent, could not be determined. This precluded a reliable relation of the determined activities to the end of irradiation time. All radionuclides observed on the anion exchange column, including the ones which were excluded from the production rate calculation, are visualized in the gamma spectrum in the Supplementary Information, Fig. S2b. The production rates obtained with this approach are presumably an underestimation as the gamma ray intensities in the spectroscopic measurements are more suppressed by the catalytic converter's metallic outer shell. The activities determined on all components are outlined in the Supplementary Information, table S3. For the metastable radionuclides $^{82m}$Rb (table 3) and $^{44m}$Sc (table 4) no *P* were predicted by the PHITS code. However, their total formation rate could be determined as 7.44(30)E-6 $^{82m}$Rb and 1.21(4)E-4 $^{44m}$Sc per incoming $^{78}$Kr.

**Table 4** The approximated total production rates ($P_{total}$) for radioactive species determined on the cation and/or anion exchange column and on the catalytic converter in comparison to the PHITS-based prediction ($P_{PHITS}$).

| **Radionuclide** | **Production** | **$t_{1/2}$ daughter/parent** | **$P_{PHITS}$ daughter/parent** | **$P_{total}$** |
|---|---|---|---|---|
| | | | **(nuclei/incoming $^{78}$Kr)** | |
| $^{44m}$Sc | $^{44m}$Sc | 2.44 d | - | 1.21(4)E-4 |
| $^{52}$Mn | $^{52}$Mn | 5.59 d | 1.01E-4 | 2.50(3)E-4 |
| $^{48}$V | $^{48}$V | 15.97 d | 2.69E-4 | 2.70(4)E-4 |
| | $^{48}$Cr → $^{48}$V | 21.6 h | 1.71E-5 | |
| $^{67}$Ga | $^{67}$Ga | 3.26 d | 1.52E-3 | 7.09(6)E-4 |
| | $^{67}$Ge → $^{67}$Ga | 18.9 min | 3.73E-4 | |
| $^{66}$Ge | $^{66}$Ge | 2.3 h | 1.52E-4 | 4.58(70)E-3 |
| $^{69}$Ge | $^{69}$Ge | 1.63 d | 1.78E-3 | 1.01(2)E-3 |
| | $^{69}$As → $^{69}$Ge | 15.2 min | 2.72E-4 | |
| $^{71}$As | $^{71}$As | 2.72 d | 2.00E-3 | 1.51(2)E-3 |
| | $^{71}$Se → $^{71}$As | 4.7 min | 2.74E-4 | |
| $^{72}$Se | $^{72}$Se | 8.40 d | 1.75E-3 | 7.37(8)E-4 |
| $^{73}$Se | $^{73}$Se | 7.2 h | 1.93E-03 | 1.25(2)E-3 |

A precise knowledge of the production rates in combination with the adsorption behaviour on the columns allows for predictions about the expected activity levels of each radionuclide in the system at any given time. The adsorption process depends on several system parameters, such as water and gas flow rates as well as column and tubing dimensions. However, offline tests performed prior to the harvesting experiment can give reasonable estimates. This information, together with the production rates, can be utilized in optimizing isotope harvesting procedures and also allows for more detailed safety and experimental planning. The discrepancies observed between the predicted and determined production rates indicate the importance of experimental measurements to allow more precise predictions of radioactivity levels. The graphical representation of the $^{62}$Zn levels on the column and in the water in fig. 2 is an exemplification of such estimations. These evaluations are even more important in future irradiations at NSCL and FIRB, where the measured rates will be extrapolated to higher beam intensities.

The $^{78}$Kr beam used in the present experiment is suitable when $^{76}$Kr is the targeted product. Lighter fragments like $^{62}$Zn are also produced with this primary beam but at a much lower production rate. At FRIB, a $^{64}$Zn beam will be available reaching the isotope harvesting beam dump at an energy of 205 MeV/nucleon and a beam intensity of 21 pμA during full power operation. Under these conditions, a 12-times higher production rate of 1.08E-3 $^{62}$Zn per incoming $^{64}$Zn is predicted, which would produce >65 GBq $^{62}$Zn in an 8 hour irradiation.[28]

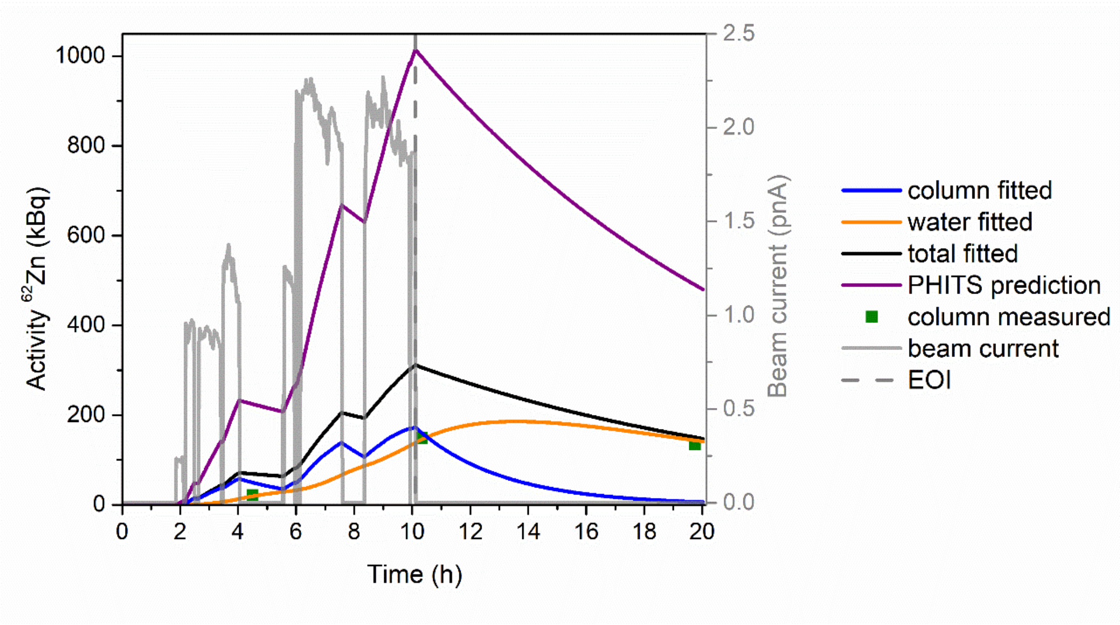

**Fig. 2** The experimentally determined (green data points) and PHITS-predicted (purple line) $^{62}$Zn levels for the $^{78}$Kr irradiation in April 2019. The quantities in the water (blue line) and on the column (orange line) were estimated by applying the determined production (9.08(30)E-5 $^{62}$Zn/ incoming $^{78}$Kr) and adsorption rate (7.19(40)E-5 $s^{-1}$). The corresponding beam current (grey line) is outlined on the secondary y-axis.

## Isolation of $^{62}$Zn and $^{62}$Cu

The first step of the separation entailed rinsing the cation exchange column with MilliQ water, by which no quantifiable amount of radioactivity was eluted. With the application of 1M HCl >96% of the $^{62}$Zn activity was eluted. In addition to $^{62}$Zn, the radionuclides $^{7}$Be, $^{24}$Na, $^{28}$Mg, $^{44g/m,47}$Sc, $^{52,56}$Mn, $^{61}$Cu, $^{63}$Zn, $^{66,67}$Ga, $^{81,82m}$Rb and $^{80,81,83}$Sr were observed in the collected eluate. Performing the elution with a less concentrated HCl solution allowed an adequate elution of $^{62}$Zn, while minimizing the desorption of other radioactive and stable contaminants.[29] After acidification, the resulting 2M HCl solution was passed over a pre-conditioned anion exchange column, on which the $^{62}$Zn activity was quantitatively adsorbed (Fig. 3). A complete removal of all accompanying radioactive contaminants was ensured by rinsing with 2M HCl, after which $^{62}$Zn represented the only radioactive species on the resin. Since no detectable levels of radioactivity could be determined in the 2M HCl rinse fraction, the volume could be reduced to a few mL in future separations.

The positron-emitter $^{62}$Zn decays with a half-life of 9.2 hours to the short-lived $^{62}$Cu ($t_{1/2}$= 9.7 min, $I_{\beta+}$= 100%), establishing a transient equilibrium between the mother and daughter radionuclide. In nuclear medicine the $^{62}$Zn/$^{62}$Cu relationship is employed as part of a radionuclide generator system, enabling the repeated isolation of a short-lived PET radionuclide.[12,13] After the successful removal of all radioactive contaminants and a short time period in which $^{62}$Cu is generated on the column, further application of 2M HCl facilitated the elution of pure, newly generated $^{62}$Cu.[30] The fast generation of $^{62}$Cu, i.e. 85% of the maximum activity are reached after an ingrowth period of only 21 minutes, allowed for subsequent elutions of the daughter within a short time period. To quantify the $^{62}$Cu in the isolated fractions, the gamma ray peak at 511 keV was monitored. In Fig 4a the independent decay of several $^{62}$Cu fractions with respect to their exact separation time points are shown. The determined activities of sample 2 and 3 are in line with the calculated decay curves, whereas the measurements of sample 1 deviate from the expected decay curve. This might be due to the interference with other positron decaying species, removed from the column into the first collected fraction. Gamma spectra of the pure $^{62}$Cu eluate (sample 2) and the anion column with $^{62}$Zn/$^{62}$Cu can be found in the Supplementary Information, Fig. S2.

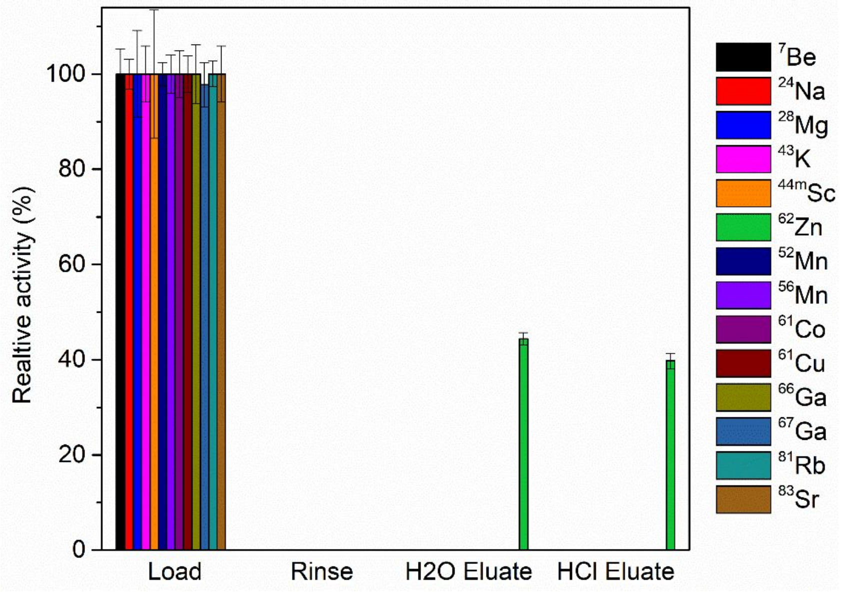

**Fig 3** Example of the elution profile from the anion exchange column. The error bars include the counting statistics and the deviations from two replicate experiments.

The following elution of zinc is facilitated by a decrease in HCl molarity, which promotes the formation of cationic species with a low adsorption on anionic resin.[30] In the first water-based fraction 44.4(13) % $^{62}$Zn was eluted, whereas an additional 39.8(16) % $^{62}$Zn was removed by the subsequently applied dilute HCl (pH~3). With the consecutive use of water and dilute HCl, a maximum elution efficiency is achieved while an increase of the pH-value and a possible formation of hydroxides could be avoided. A comparable elution behaviour on AG1x8 resin is reported by Zweit et al, attaining an elution efficiency of 96% by using 40 mL water.[16] The total recovery yield of the $^{62}$Zn isolation, including the elution from the cation exchange resin, amounted to 83.3(49) %, whereas an overall recovery yield, considering also the collection from the water of the harvesting system, of 80.5(52) % was attained. The volume of the obtained $^{62}$Zn eluate was reduced by evaporation and the activity was quantitatively reconstituted in 0.01M HCl. The isolated $^{62}$Zn was of high radionuclidic purity, with the daughter $^{62}$Cu being the only accompanying radionuclide above the limit of detection with the used gamma spectrometer.

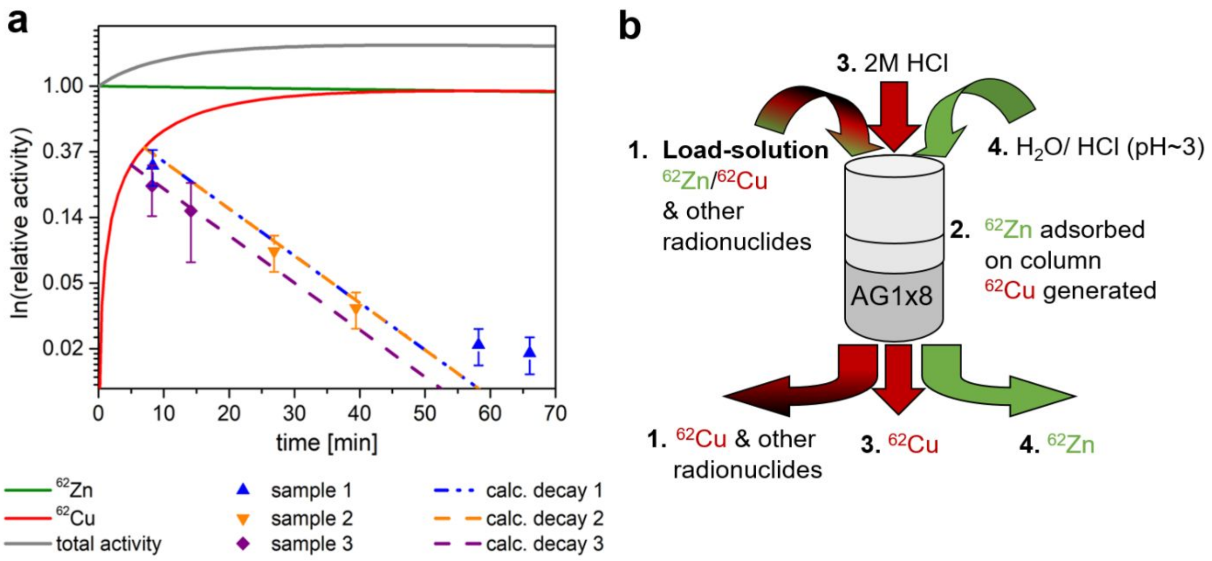

**Fig 4** (**a**) The transient equilibrium established by the decay of the parent nuclide $^{62}$Zn to the daughter nuclide $^{62}$Cu (solid green and red line), reaching the maximum $^{62}$Cu activity after 36 minutes. The decay of the isolated $^{62}$Cu fractions was followed by gamma spectroscopy (single data points) while the dashed lines represent the calculated decay behaviour. The error bars result from the statistical uncertainties in the detection method. (**b**) Schematic of the purification and generator elution process. The order of the individual steps of the process are indicated by numbers.

### Uptake of $^{62}$Zn by garden cress

With a purified sample of $^{62}$Zn in-hand, it was possible to assess its biological applicability by performing a simple experiment in a garden cress culture. In many plant systems, the uptake of zinc is believed to be mainly mediated as divalent cation ($Zn^{2+}$). However, a contribution from organic Zn complexes has been observed in some vegetable plants. Investigations into the associated metabolomic pathways utilize organic chelators with stable and/or radioactive isotopes of zinc to trace uptake behaviour.[22–25] For the present case, the decay characteristics of $^{62}$Zn were considered suitable for a proof-of-principle uptake study in garden cress using ligand-free and DTPA-radiolabelled $^{62}$Zn. The garden cress was hydroponically grown in water and on moist cotton, which are both frequently utilized growth media.[31,32] Hydroponic culture methods are commonly used for studies of metal plant uptake, as solutions are chemically better defined and more homogeneous than soils.[23] The uptake was followed by phosphor imaging which was performed from 8.5 h to 93 h post incubation. Representative phosphor images of garden cress plants are shown in Fig. 5 a and b. The recorded signal intensities were used to compare the percentage of absorbed ligand-free $^{62}$Zn with the absorbed chelated $^{62}$Zn. A correction of the signal intensities with respect to the film exposure time and the $^{62}$Zn decay was not necessary, given that intensities were compared between samples exposed on the same film (where both the exposure time and the decay were the same). In the resulting graphical representation (Fig. 6 a and b), a percentage higher than 50 indicates the extent to which ligand-free $^{62}$Zn is preferably absorbed over DTPA-labelled $^{62}$Zn (A more in depth explanation about the processing of the raw data is given in the Experimental.) Stable zinc chloride was added at a low concentration to several dishes to prevent an unspecific adsorption to surfaces and precipitation of radio-zinc.

The growth of garden cress was used as an indicator for any adverse effects due to the applied incubation solutions. The suitability of the chosen experimental conditions was demonstrated by the comparable plant heights between the control and experimental dishes (Supplementary Information, Fig. S4).

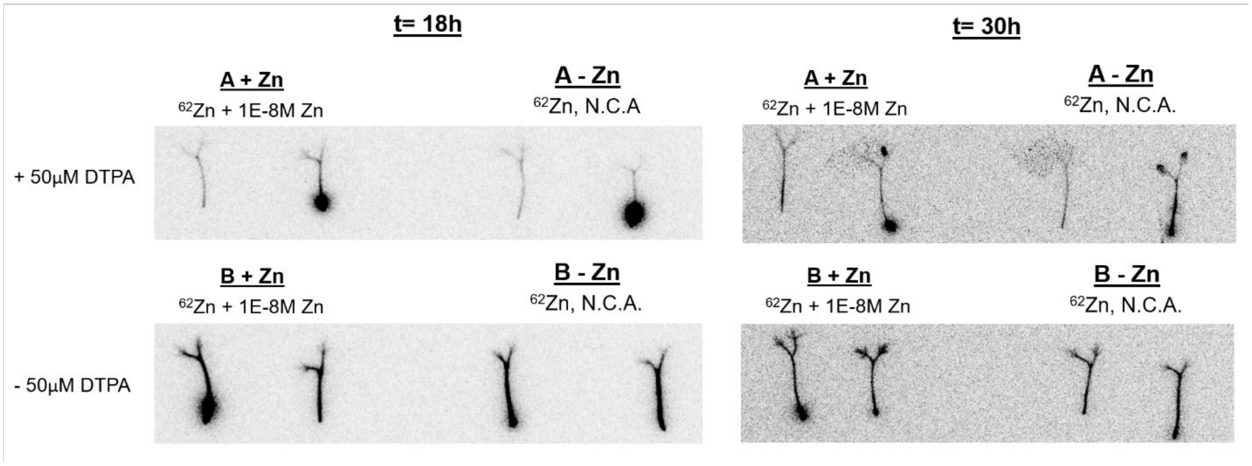

**Fig. 5** Phosphor images of garden cress harvested after 18 h and 30 h of incubation with ligand-free and DTPA-labelled $^{62}$Zn. The exact composition of the incubation solutions is given in table 2. (Note: zinc deficient (-Zn) samples are labelled as N.C.A., no carrier added, which denotes that no stable carrier element has been added.) The higher signal intensities in roots of several plants (visualized in the second and fourth plant in the upper row) can be explained by the surface adsorption of $^{62}$Zn where the plants were in direct contact with the solution. These areas were not considered for determining the signal intensity.

In the cotton-cultivated garden cress a preferred absorption of ligand-free $^{62}$Zn could be observed, with the highest assimilation at the earliest time point (t~10 hours). With prolonged incubation times (38–93 h), the percentage metric for $^{62}$Zn uptake decreased from 79% to 54%. The largely comparable $^{62}$Zn uptake in zinc-supplied (+Zn) and zinc-deficient (-Zn) samples suggests a homogenous radio-zinc distribution (Fig. 6 a). For the water-grown cress a trend towards a favoured ligand-free $^{62}$Zn uptake was only discernible in the non-supplemented samples. A prevailing radiochemical equilibrium of $^{62}$Zn and $^{62}$Cu can be assumed in the incubation solution and consequentially also for the plant uptake. However, due to the short half-life of $^{62}$Cu the effect of the direct $^{62}$Cu uptake on the observed signal intensities was expected to be negligible. The $^{62}$Zn assimilated in the garden cress plants is in radiochemical equilibrium with its daughter radionuclide $^{62}$Cu. Here both radionuclides contribute to the observed signal intensities, but the short half-life of $^{62}$Cu precludes a distribution different to that of its parent $^{62}$Zn. Therefore, $^{62}$Zn was the only mentioned radionuclide within the context of the plant uptake and imaging experiments.

The preferable absorption of unchelated $^{62}$Zn in cotton-grown cress and the zinc-deficient samples of water-grown cress would point towards an uptake mechanism mainly mediated by the divalent cation. This would support the commonly assumed hypothesis that the free metal activity determines the uptake of trace metals, rather than being stimulated by metal complexes as demonstrated in studies with lettuce and spinach.[19,22,23] However, the herein presented results are the summary of only two experiments, where the uptake at each time point was assessed just once. To corroborate these preliminary findings and also to elucidate the influence of different incubation conditions and growth-media, a more exhaustive study with a larger sample size would be necessary. The implementation of quantitative imaging would additionally allow the assessment of the absolute amount of adsorbed zinc. Nevertheless, the present experiment demonstrated the feasibility of using $^{62}$Zn as an imaging agent to estimate the zinc uptake in a hydroponic garden cress culture. Additionally, it underlines the possibility to extend the use of diverse radiometals, harvested at heavy ion beam facilities, to plant biology studies.

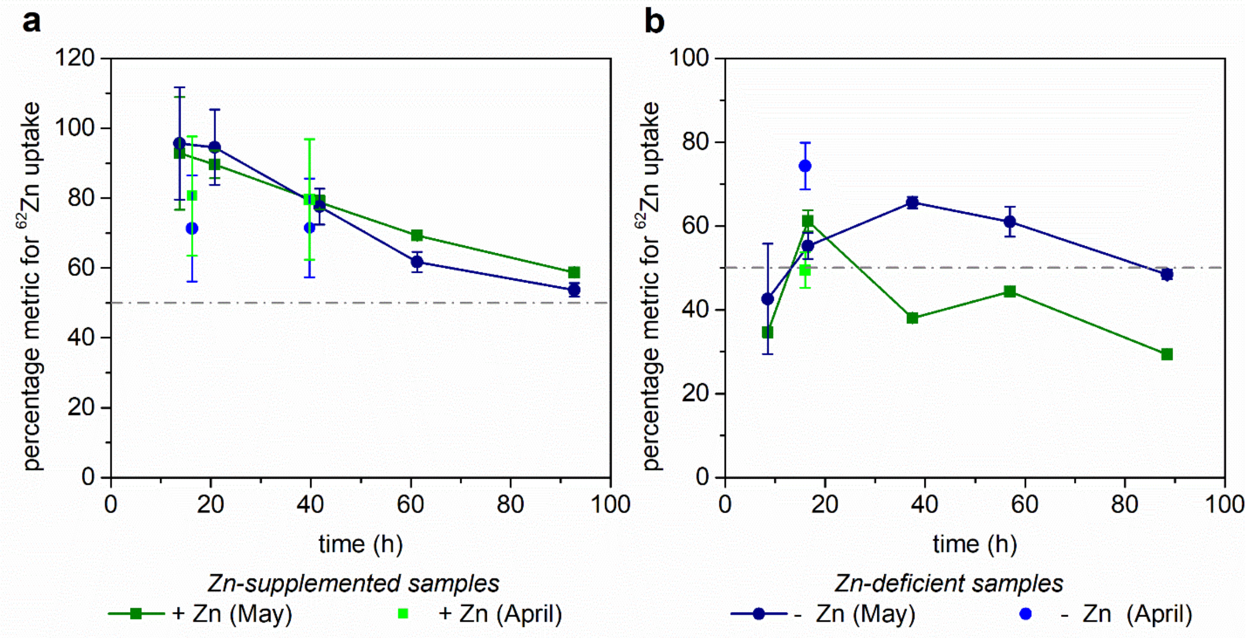

**Fig. 6** Uptake of $^{62}$Zn by garden cress cultivated on (**a**) a layer of cotton and (**b**) in water. A set of samples was supplied with stable zinc chloride (Zn-supplemented samples, indicated by + Zn and green data points) while another one set did not receive any additional zinc (Zn-deficient samples, indicated by- Zn and blue data points). The error bars represent the difference between the individually imaged garden cress seedlings (n=2-3) harvested from one petri dish.

## Conclusion

The feasibility of collecting the aqueous radionuclide $^{62}$Zn in the background of a $^{76,77}$Kr collection was demonstrated at the NSCL. In addition to the production rate of $^{62}$Zn (9.08(30)E-5 $^{62}$Zn per incoming $^{78}$Kr), the rates of formation of eleven other cationic radionuclides could be determined and compared with the predicted values. The radiochemical separation on an anion exchange resin yielded a $^{62}$Zn eluate of high radionuclidic purity. The diverse applicability of the radionuclide pair $^{62}$Zn/$^{62}$Cu was first demonstrated by the radiogenerator principle with the isolation of pure $^{62}$Cu. By applying this method to larger quantities of $^{62}$Zn/$^{62}$Cu, a yet untapped source of this radiopharmaceutically interesting PET-radionuclide could become available. Secondly, the obtained $^{62}$Zn was utilized in a proof of principle plant uptake study. The $^{64}$Zn beam of the upcoming FRIB could contribute to a considerably improved $^{62}$Zn production, where GBq amounts would be available for applications ranging from plant biology to nuclear medicine.

## Acknowledgement

The authors would like to thank Dr. Thomas Baumann, Prof. Dave Morrisey, Dr. Matthias Steiner and Prof. Andreas Stolz for providing and tuning the $^{78}$Kr beam. Additionally, we would like to acknowledge the support of Nicholas Dronchi and Chloe Kleindfeldt during the $^{78}$Kr beam experiment. We wold also like to thank Dali Georgobiani for performing the production rate simulations with the PHITS code.

## Funding

This research is supported by the U.S. Department of Energy Isotope Program, managed by the Office of Science for Isotope R&D and Production (DE-SC0018637). Additional support was provided by the U.S. Department of Energy National Nuclear Security Administration Stewardship Science Graduate Fellowship, United States (DENA0003864) program and Michigan State University, United States.

## References

1 T. Mastren, A. Pen, S. Loveless, B. V. Marquez, E. Bollinger, B. Marois, N. Hubley, K. Brown, D. J. Morrissey, G. F. Peaslee and S. E. Lapi, *Anal. Chem.*, 2015, **87**, 10323–10329.

2 E. P. Abel, M. Avilov, V. Ayres, E. Birnbaum, G. Bollen, G. Bonito, T. Bredeweg, H. Clause, A. Couture, J. DeVore, M. Dietrich, P. Ellison, J. Engle, R. Ferrieri, J. Fitzsimmons, M. Friedman, D. Georgobiani, S. Graves, J. Greene, S. Lapi, C. S. Loveless, P. Mantica, T. Mastren, C. Martinez-Gomez, S. McGuinness, W. Mittig, D. Morrissey, G. Peaslee, F. Pellemoine, J. D. Robertson, N. Scielzo, M. Scott, G. Severin, D. Shaughnessy, J. Shusterman, J. Singh, M. Stoyer, L. Sutherlin, A. Visser and J. Wilkinson, *Isotope Harvesting at FRIB: Additional opportunities for scientific discovery*, 2018.

3 E. P. Abel, H. K. Clause and G. W. Severin, *Appl. Radiat. Isot.*, 2020, **158**, 109049.

4 K. A. Domnanich, E. P. Abel, H. K. Clause, C. Kalman, W. Walker and G. W. Severin, *Nucl. Instruments Methods Phys. Res. Sect. A Accel. Spectrometers, Detect. Assoc. Equip.*, 2020, **959**, 163526.

5 A. Pen, T. Mastren, G. F. Peaslee, K. Petrasky, P. A. Deyoung, D. J. Morrissey and S. E. Lapi, *Nucl. Instruments Methods Phys. Res. Sect. A Accel. Spectrometers, Detect. Assoc. Equip.*, 2014, **747**, 62–68.

6 C. S. Loveless, B. E. Marois, S. J. Ferran, J. T. Wilkinson, L. Sutherlin, G. Severin, J. A. Shusterman, N. D. Scielzo, M. A. Stoyer, D. J. Morrissey, J. D. Robertson, G. F. Peaslee and S. E. Lapi, *Appl. Radiat. Isot.*, 2020, **157**, 109023.

7 T. Mastren, A. Pen, G. F. Peaslee, N. Wozniak, S. Loveless, S. Essenmacher, L. G. Sobotka, D. J. Morrissey and S. E. Lapi, *Sci. Rep.*, 2014, **4**, 1–6.

8 M. J. Rowland, D.J., McCarthy, M.J., Welch, in *Handbook of Radiopharmaceuticals: Radiochemistry and Applications*, John Wiley & Sons Ltd, New York, NY, 2003, pp. 441–465.

9 M. J. Adam and D. S. Wilbur, *Chem. Soc. Rev.*, 2005, **34**, 153–163.

10 International Atomic Energy Agency, Nuclear Data Services, https://www-nds.iaea.org/, (accessed 23 April 2020).

11 T. Sato, Y. Iwamoto, S. Hashimoto, T. Ogawa, T. Furuta, S. ichiro Abe, T. Kai, P. E. Tsai, N. Matsuda, H. Iwase, N. Shigyo, L. Sihver and K. Niita, *J. Nucl. Sci. Technol.*, 2018, **55**, 684–690.

12 A. Dash and R. Chakravarty, *Am. J. Nucl. Med. Mol. Imaging*, 2019, **9**, 30–66.

13 T. Z. Wong, J. L. Lacy, N. A. Petry, T. C. Hawk, T. A. Sporn, M. W. Dewhirst and G. Vlahovic, *Am. J. Roentgenol.*, 2008, **190**, 427–432.

14 H. Kurihara, *Oncotarget*, 2018, **9**, 31165–31166.

15 Y. Ng, J. Lacy, J. Fletcher and M. Green, *Appl. Radiat. Isot.*, 2014, **91**, 38–43.

16 J. Zweit, R. Goodall, M. Cox, J. W. Babich, G. A. Potter, H. L. Sharma and R. J. Ott, .

17 G. Bormans, A. Janssen, P. Adriaens, D. Crombez, A. Witsenboer, J. de Goeij, L. Mortelmans and A. Verbruggen, *Int. J. Radiat. Appl. Instrumentation. Part*, 1992, **43**, 1437–1441.

18 J. Avery, Stephens; Yue, Zhiwei; Bui, Huong; Thrash, Thomas; Martin, Chris; Lacy, *Jorunal Nucl. Med.*

19 N. Gupta, H. Ram and B. Kumar, *Rev. Environ. Sci. Biotechnol.*, 2016, **15**, 89–109.

20 A. Sharma, B. Patni, D. Shankhdhar and S. C. Shankhdhar, *Physiol. Mol. Biol. Plants*, 2013, **19**, 11–20.

21 M. R. Broadley, P. J. White, J. P. Hammond, I. Zelko and A. Lux, *New Phytol.*, 2007, **173**, 677–702.

22 M. Mclaughlin, E. Smolders, R. Merckx and A. Maes, 1997, 113–118.

23 A. F. Degryse, E. Smolders, D. R. Parker and S. Plant, 2019, **289**, 171–185.

24 R. N. Collins, G. Merrington, M. J. McLaughlin and C. Knudsen, *Environ. Toxicol. Chem.*, 2002, **21**, 1940–1945.

25 Å. R. Almås and B. R. Singh, *J. Environ. Qual.*, 2001, **30**, 869–877.

26 A. Gade and B. M. Sherrill, *Phys. Scr.*, , DOI:10.1088/0031-8949/91/5/053003.

27 E. P. Abel, K. Domnanich, C. Kalman, W. Walker, J. W. Engle, T. E. Barnhart and G. Severin, *Nucl. Instruments Methods Phys. Res. Sect. B Beam Interact. with Mater. Atoms*, 2020, **478**, 34–45.

28 O. B. Tarasov and D. Bazin, *Nucl. Instruments Methods Phys. Res. Sect. B Beam Interact. with Mater. Atoms*, 2008, **266**, 4657–4664.

29 F. W. E. Strelow, 1984, 1053–1056.

30 Johannes Korkisch, *Handbook of Ion Exchange Resins: Their Application to Inorganic Analytical Chemistry*, CRC Press Inc., Boca Raton, Florida, 1989.

31 H. M. Resh, *Hydroponic Food Production*, CRC Press Inc., Boca Raton, Florida, 7th ed., 2012.

32 D. B. Munro and E. Small, *Vegetables of Canada*, NRC Research Press, Ottawa, 1997.